

# Dark Channel-Assisted Depth-from-Defocus from a Single Image

Moushumi Medhi and Rajiv Ranjan Sahay

**Abstract**—In this paper, we utilize the dark channel as a complementary cue to estimate the depth of a scene from a single space-variant defocus blurred image due to its effectiveness in implicitly capturing the local statistics of blurred images and the scene structure. Existing depth-from-defocus (DFD) techniques typically rely on multiple images with varying apertures or focus settings to recover depth information. Very few attempts have focused on DFD from a single defocused image due to the under-constrained nature of the problem. Our method capitalizes on the relationship between local defocus blur and contrast variations as key depth cues to enhance the overall performance in estimating the scene’s structure. The entire pipeline is trained adversarially in a fully end-to-end fashion. Experiments conducted on real data with realistic depth-induced defocus blur demonstrate that incorporating dark channel prior into single image DFD yields meaningful depth estimation results, validating the effectiveness of our approach.

**Index Terms**—Depth-from-defocus, dark channel, local variation map.

## I. INTRODUCTION

DEPTH-FROM-DEFOCUS from a single input aims at estimating the scene depth from a single out-of-focus image. A single defocused image, captured instantly by a system or robot without relying on autofocus, can provide fast depth cues. Naturally occurring blur from optical limitations can be leveraged as an advantage, enabling depth extraction in situations where conventional all-in-focus methods falter. This paper presents a novel method to estimate depth from a single defocused blurred image captured with a fixed aperture setting. Existing depth from defocus (DFD) methodologies [1]–[9] tend to rely on multiple images collected with varying apertures or focus configurations to derive depth information. These methods exploit the defocus relationship observed among the images with differing focal settings. For instance, [5] jointly trains two networks, DefocusNet and FocusNet, where DefocusNet processes a defocused image to predict depth, which is then used with an input all-in-focus (AIF) image to generate a synthetic focal stack. FocusNet, in turn, estimates depth from this focal stack, and its output is combined with the AIF image to reconstruct the defocused image. During training, the networks leverage depth and defocus image consistency losses for self-supervision, but at inference, depth estimation can be performed either from a single defocused image or from a focal stack. Unlike these works, which rely on video sequences, multiple frames during either training or inference, or the fusion of multiple cues and traditional optimization techniques, our study explores

M. Medhi is in the Advanced Technology Development Center, Indian Institute of Technology, Kharagpur, India, 721302. e-mail: medhi.moushumi@iitkgp.ac.in

R. R. Sahay is with department of Electrical Engineering, Indian Institute of Technology, Kharagpur, India, 721302.

deep learning-based and a novel dark channel-based method to address the ill-posed problem of single image DFD, where only a single defocused image is used during both training and testing. This distinction is critical, as our approach is designed for scenarios where only a single image is available, such as monocular imaging systems, making it fundamentally different and challenging compared to prior video-based or multi-cue methods.

While multi-image DFD techniques often outperform single-image approaches, single-image DFD remains a significantly more constrained and challenging task. Comparatively, limited research [10]–[13] has addressed DFD using a single defocused image, given the challenging nature of the problem. These methods [10]–[13] utilized end-to-end neural networks to estimate depth maps in a supervised learning setting using ground truth depth data. To enhance the DFD results, [10] additionally computed blur kernels for deblurring, while [12] derived lens parameters (blur factor and focus disparity) for defocus blur estimation from the predicted depth map. [14] estimates depth from a single all-in-focus (AIF) image as input and leverages the defocused image solely for supervision during training. In another instance of depth estimation from AIF image [15], a transmission map, computed from the dark channel, has been employed as a fourth channel input to a network. In this study, we propose a novel approach to leveraging the relationship between local defocus blur and contrast variations using dark channel to deduce the presence and extent of defocus blur, providing clues for depth estimation. Dark channel prior (DCP) has been popularly used to estimate depth from hazy/foggy/underwater images [16]–[18], where DCP was exploited to compute the scene transmission map which is a function of depth. However, DCP has also been recently adapted for space-variant blur analysis for deblurring [19]–[21] based on sparsity of dark channel in deblurred images. Although defocus blur degradation is a result of the camera’s optical effects, unlike optical scattering in the physical medium due to haze/fog, the dark channel plays an analogous role in both types of degraded images. In defocused blurred images, regions near the focal plane generally exhibit reduced blur. The dark channel accentuates these regions because of their increased intensity variability. Conversely, the dark channel exhibits reduced intensity variance in significantly blurred areas distant from the focal plane and also lacks sharp details due to the smoothing effect of the blur. We have leveraged the combined local intensity deviation of both the defocused image and its dark channel, namely, the Local Defocus and Dark Channel Variation (LDDCV) map, to improve DFD performance. The Kernel Density Estimate (KDE) plot for NYU-Depth V2 (NYU-v2) dataset [22] in Fig. 1 helps in visualizing how the dark channel intensity discrepancy and the LDDCV map difference change with normalized spatially

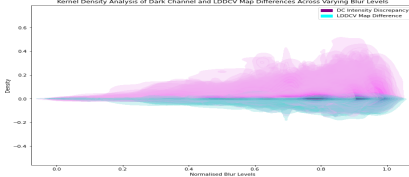


Fig. 1. Kernel Density Estimate (KDE) plot for NYU-Depth V2 dataset [22].

varying blur level, which is a function of scene depth. Additionally, we have used an adversarial network to supervise our DFD model using defocus blur map as an adversarial supervisory signal during training. Our single-image DFD approach also offers a promising alternative to traditional multi-image or hardware-intensive methods, enabling rapid depth inference from limited data to improve system efficiency. A system could be engineered to deliberately operate with a fixed focus, wide aperture (which naturally induces defocus blur) camera to passively infer depth from a single shot. This approach reduces system complexity and cost compared to the active depth sensing technique, making it a practical and scalable solution for real-world automation applications. Our empirical results show that applying DCP to defocused images yields meaningful depth estimation results.

## II. PROPOSED APPROACH

### A. Dark Channel and LDDCV Map as Complementary Cues

We compute the darkest scene radiance  $J_{df}$  of the defocused image  $I_{df}$  from the minimum intensity value among the three color channels  $c$  (Red  $r$ , Green  $g$ , Blue  $b$ ) in a local window of size  $\Omega(i) \times \Omega(i)$  centered around pixel  $i$  of  $I_{df}$  as

$$J_{df}(I_{df})(i) = \min_{p \in \Omega(i)} \left( \min_{c \in \{R, G, B\}} I_{df}^c(p) \right) \quad (1)$$

The dark channel emphasizes the length of shadows, edges, and darker structural elements, which can provide additional context for understanding the 3D layout of the scene in a non-conventional way, such as spatial arrangement and relative distances between objects in a scene. Despite the inherent loss of information in terms of fine textures and details, the dark channel retains the major scene structure and the edges, which correspond to significant depth transitions. This can sometimes lead to better clarity of larger structural elements as it reduces noise and smooths out small variations. We have integrated the features extracted from the single defocus image with those of the dark channel to obtain enhanced structural information for the depth estimation model.

The Local Defocus and Dark Channel Variation (LDDCV) map is a dual-channel intensity variation map obtained by concatenating the Local Defocus Variation (LDV) and the Local Dark Channel Variation (LDCV) maps. They depict the maximum intensity deviation among neighboring pixels within a local region and form adequate representations by capturing the subtleties of depth-dependent defocus blur. The

LDV and LDCV maps highlight the local variations in  $I_{df}$  and  $J_{df}$ , respectively. Mathematically,

$$\begin{aligned} LDDCV(J, I)(i, j) = & \{ \max |J(i, j) - J(p, q)|, \\ & \max |I(i, j) - I(p, q)| \mid p = i-1, i, i+1, q = j-1, j, j+1 \} \end{aligned} \quad (2)$$

The presence of defocus blur smooths the overall appearance of the image by reducing the sharp variations and lowering the maxima values within local regions. Due to the homogenizing effect of defocus blur in the local regions, areas with high defocus blur show lower local variations in the LDDCV map. On the contrary, regions with low-defocus blur show slightly higher LDDCV values. This observation can be used to determine the presence and extent of defocus blur in the image and to offer insights to assess the depth of a single out-of-focus image.

### B. Network Architecture

The schematic architecture of our network is illustrated in Fig. 2. For a given defocus image  $I_{df} \in \mathbb{R}^{H \times W \times 3}$ , a pretrained ResNeXt101-32x8d-wsl [23] is employed as the encoder backbone (labeled (a) in Fig. 2), leveraging the multiscale features  $F_i^{df} \in \mathbb{R}^{H_i \times W_i \times C_i}$  from different encoder layers  $i$  ( $i = 1, 2, 3, 4$ ). Here,  $H_i$ ,  $W_i$ , and  $C_i$  denote the height, width, and channel dimension, respectively. Similarly, multiscale features  $F_i^l \in \mathbb{R}^{H_i \times W_i \times C_i'}$  are extracted from the LDDCV embedding network (LDDCV-Net), labeled as (b). Additionally, a parallel mask-mediated sparse pooling network (MMSP-Net) (labeled (c)) is employed to extract multiscale pooled features  $F_i^{lv} \in \mathbb{R}^{H_i \times W_i \times C_i''}$  from the input LDDCV map and its validity mask (1 if  $|LDDCV| > T$ , where  $T = 0.05$  is the threshold), which are then concatenated with  $F_i^l$ . The structural information highlighted by the dark channel  $J_{df}$  is embedded into a latent space (labeled (d)) by a dark channel embedding network (D-Net) before passing through a global average pooling (GAP) and then flattened to obtain features  $z \in \mathbb{R}^{1 \times Q}$ . The Nested Feature Modulation and Fusion Module ( $Nest(FM)^2$ ), marked as (e), is structured into nested, multi-layered groups to extract nuanced cues from the embedded dark channel features  $z$  that modulate the primary features  $F^b \in \mathbb{R}^{\eta_{h_i} \times \eta_{w_j} \times Q}$  in a hierarchical manner. The nested repetition of ARU, Core Feature Transformation Block (CFTB), Multi-level Feature Enhancement Block (MFEB), and Hierarchical Residual Refinement ( $HR^2B$ ) facilitates extensive feature extraction and refinement across multiple levels. The Dark channel-Infused Feature Boosting (DIFB) unit is shown in Fig. 3. We found that setting  $N$  repetitions to 2 achieves a balance between memory efficiency and DFD performance. A subsequent residual module containing a Depthwise Separable Asymmetric-Multiscale Pyramid Fusion (DSA-MSPF) block (marked as (f)) consolidates the learned representations by acting as a multi-scale context aggregation prior before passing it to the decoder (labeled (g)) for depth,  $d$ , reconstruction. We adopted the blueprint separable convolutions (BSConv) [24] throughout the entire depth generator model to reduce our model parameters by  $\approx 49\%$ . A discriminator  $D$  (labeled (h)) takes the ground truth/estimated

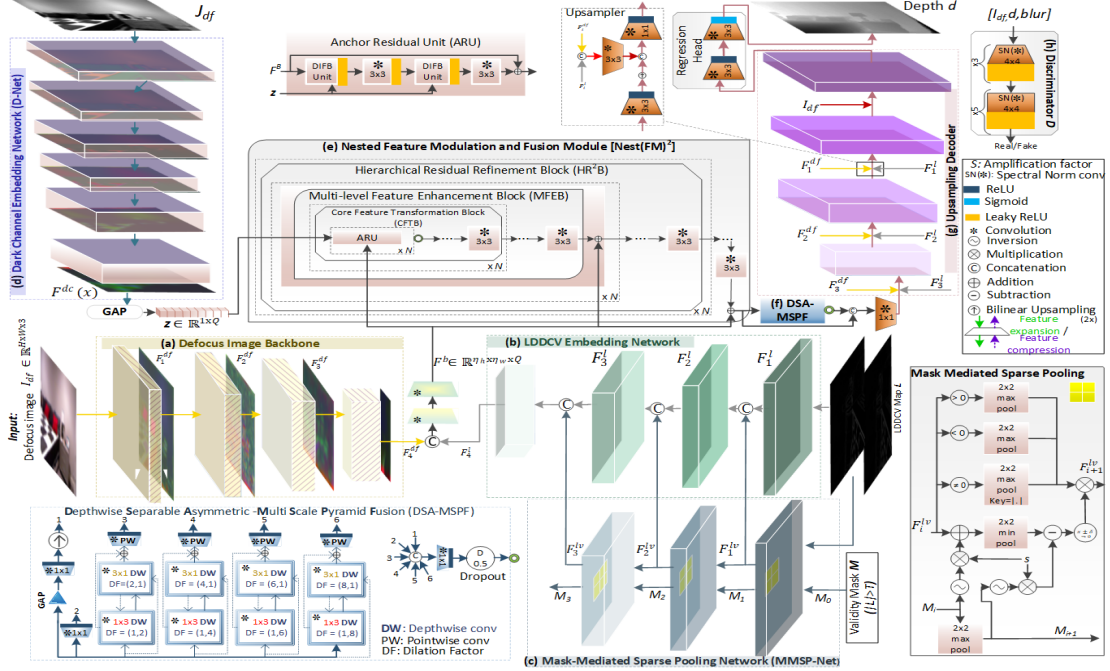


Fig. 2. Comprehensive overview of our dark channel-assisted DFD Framework. Zoom in for a clearer view of the modules.

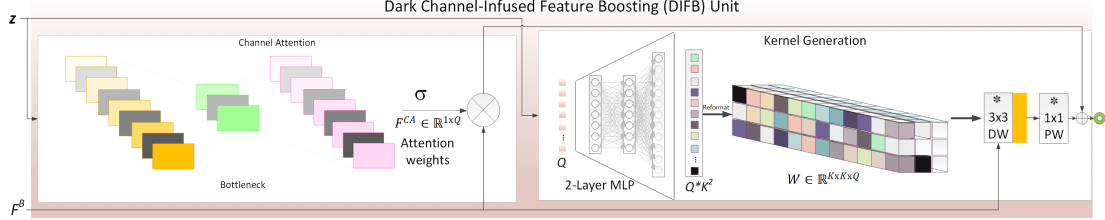


Fig. 3. Schematic architecture of the Dark channel-Infused Feature Boosting (DIFB) unit.

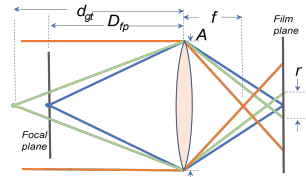


Fig. 4. A thin lens approximation model for defocus blur formation.

depth map  $d_{gt}/d$ , ground truth/estimated defocus blur map  $r(d_{gt})/r(d)$  (explained in section III-A), and the defocused image  $I_{df}$  as inputs during adversarial training to distinguish between real and generated data, respectively.

### C. Objective Function

The objective function to regress pixel-wise depth values consists of a spatial fidelity loss  $\mathcal{L}_{\text{spafid}} = |d - d_{gt}|_1$ , frequency domain loss  $\mathcal{L}_{\text{freq}} = |\text{DCT}(d) - \text{DCT}(d_{gt})|_1$ , and adversarial loss  $\mathcal{L}_{\text{adv}} = 0.5 \cdot \mathbb{E}_{d \sim p_d} [(D(d, r(d), I_{df}) - 1)^2]$  terms. The Discrete Cosine Transform (DCT) is defined as:  $\text{DCT}(x_i) = x_k \sum_{i=0}^{L-1} x_i \cos \left[ \frac{\pi}{L} \left( i + \frac{1}{2} \right) k \right]$ , where  $L$  is the total number of data points in the signal,  $k$  is the index of the DCT coefficients being calculated.  $\mathbb{E}_{d \sim p_d}$  denotes the expected

value over the distribution  $p_d$  of predicted depth map  $d$ . The joint loss function is formulated as:

$$\mathcal{L}_{\text{total}} = \mathcal{L}_{\text{spafid}} + 0.1 \cdot \mathcal{L}_{\text{freq}} + 0.1 \cdot \mathcal{L}_{\text{adv}} \quad (3)$$

## III. EXPERIMENTAL

### A. Dataset

**NYU-Depth V2 (NYU-v2) dataset** [22]: The NYU-v2 dataset [22] comprises 1,449 pairs of spatially matched RGB and depth images acquired using a Microsoft Kinect. In line with prior works [6], [11], we adopt the standard train/test eigen split consisting of 795/654 images. To generate optically realistic depth-dependent defocus effects in AIF NYU-v2 RGB image  $I$ , we select the parameters corresponding to a synthetic camera with a focal length ( $f$ ) of 9mm, an in-focus plane ( $D_{fp}$ ) at 0.7m, an F-number ( $F_n$ ) of 2 to achieve a shallow Depth of Field (DoF), sensor size  $p_x$  of 7.5 $\mu$ m, and aperture  $A = f/F_n$ . We generate the defocus blurred image  $I_{df}$  by convolving the AIF image  $I$  with a point spread function (PSF)  $G(x, y, r)$  with kernel radius  $r$  and location indices  $x, y$ :

$$I_{df}(x, y) = G(x, y) * I(x, y), G(x, y) = \frac{1}{2\pi r^2} e^{-\frac{1}{2} \frac{x^2 + y^2}{r^2}} \quad (4)$$

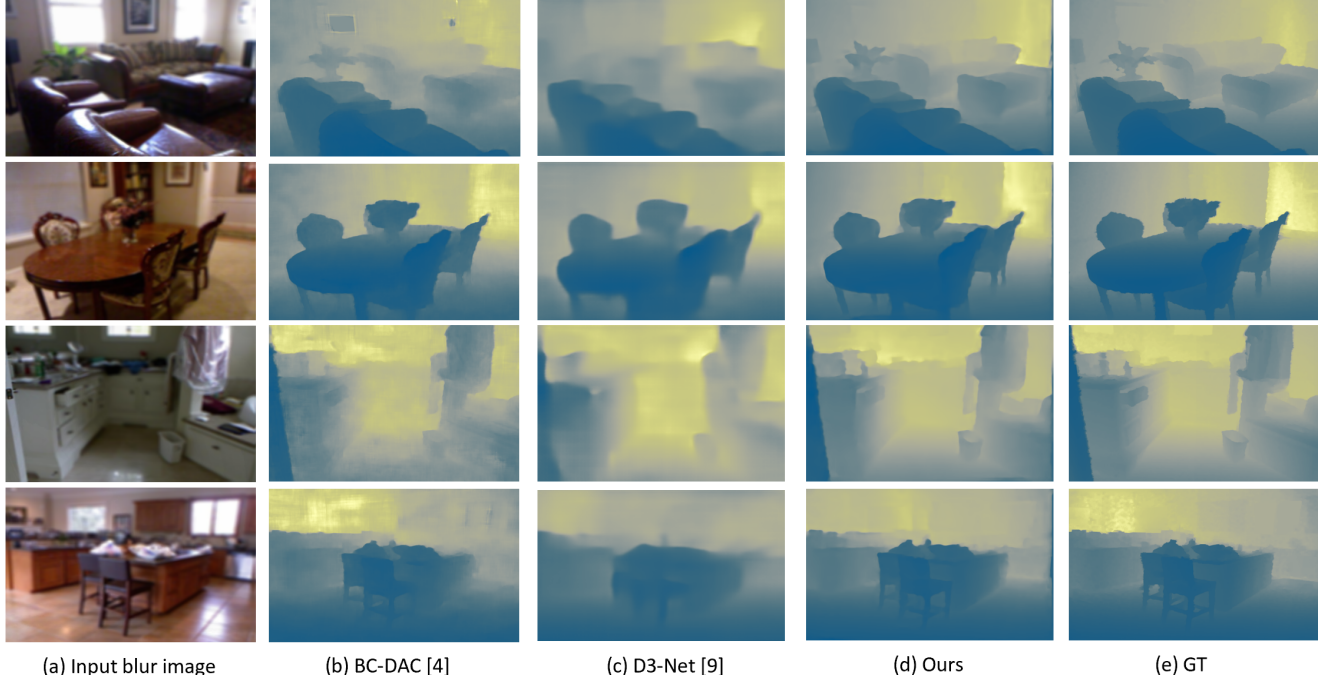


Fig. 5. Depth estimation results on four synthesized defocused blur images (a) from NYU-v2 dataset [22]. Estimated depth maps (b)-(d) along with the ground truths (GT) (e).

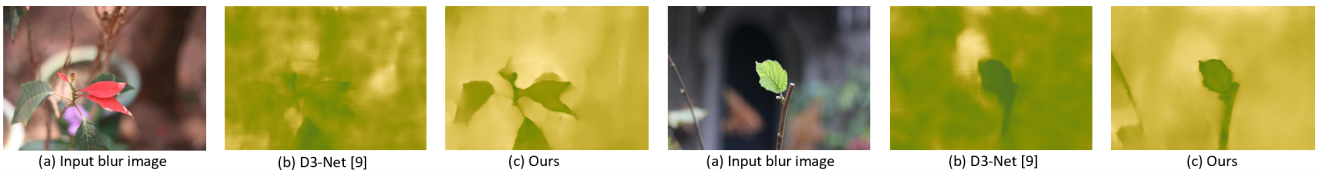


Fig. 6. Depth estimation results on two high-resolution real defocused blur images (a) from the EBD dataset [25] without fine-tuning.

TABLE I

QUANTITATIVE DEPTH ESTIMATION RESULTS ON NYU-v2 DATA [22].  
 $S_{blur}$  INDICATES TRAINING SUPERVISION FROM DEFOCUS BLUR MAP.  
 THE **BOLD** ENTRIES DENOTE THE BEST SCORES.

Methods	$S_{blur}$	Abs Rel $\downarrow$	Sq Rel $\downarrow$	RMSE [m] $\downarrow$	$logRMSE \downarrow$	$\delta_1 \uparrow$	$\delta_2 \uparrow$	$\delta_3 \uparrow$
<i>All-In-Focus (AIF) image(s)</i>								
P3Depth [26]	No	0.104	-	0.356	-	0.898	0.981	0.996
Marigold [27]	No	<b>0.055</b>	-	<b>0.224</b>	-	<b>0.964</b>	<b>0.991</b>	<b>0.998</b>
<i>Focal stack</i>								
SSDC [7]	Yes	0.170	-	0.325	-	0.950	0.979	0.987
<i>Dual defocused images</i>								
BC-DAC [6]	No	0.026	0.007	0.140	0.018	0.995	0.998	0.999
<i>Single defocused image</i>								
D3Net [11]	No	0.104	0.056	0.384	0.057	0.923	0.987	0.996
Camind [13]	Yes	0.242	0.248	0.798	0.253	0.601	0.917	0.990
Ours	Yes	<b>0.042</b>	<b>0.019</b>	<b>0.240</b>	<b>0.032</b>	<b>0.975</b>	<b>0.995</b>	<b>0.999</b>

Following the thin-lens model shown in Fig. 4,  $r$  is calculated as a function of the scene's distance,  $d_{gt}$ , from the camera as:

$$r(d_{gt}) = \frac{1}{\sqrt{2} \cdot p_x} \frac{Af}{(D_{fp} - f)} \frac{|d_{gt} - D_{fp}|}{d_{gt}} \quad (5)$$

**EBD dataset [25]:** The EBD dataset [25] contains 1,305 high-resolution ( $1600 \times 1024$ ) real defocused images without ground-truth depth map annotations. These images feature a shallow DoF with an  $F_n$  of 1.8. Note that we have used the EBD dataset [25] solely for testing.

## B. Quantitative and Qualitative Results

To quantitatively evaluate the depth estimation results, we show comparison in Table I for 4 categories of input methods in terms of 7 metrics that are widely used for depth estimation: Absolute Relative Error ( $AbsRel$ ), Square Relative Error ( $SqRel$ ), Root Mean Squared Error ( $RMSE$ ), logarithmic Root Mean Squared Error ( $logRMSE$ ), and thresholded accuracies ( $\delta_1 < 1.25$ ,  $\delta_2 < 1.25^2$ ,  $\delta_3 < 1.25^3$ ). For fair comparison, we trained and tested D3Net<sup>1</sup> [11] and Camind<sup>2</sup> [13] using our dataset. We would like to mention here that in contrast to the original work in [13], which reported test results on NYU-v2 data within a distance range of 2 m, our evaluation included the full range (10 m) of the data. This could account for the performance discrepancy, possibly explaining the lower error rates the authors reported in their paper. The results reported for BC-DAC [6] in Table I and Fig. 5 were provided by the authors. It is evident that in most of the evaluation metrics, our method demonstrates superior performance compared to the existing state-of-the-art methods that employ single defocus input [11], [13], focal stack input [7], and AIF input [26], [27]. Fig. 5 shows the qualitative results. While the outputs of BC-DAC [6] exhibit noticeable artifacts, the method occasionally

<sup>1</sup>[https://github.com/marcelampc/d3net\\_depth\\_estimation](https://github.com/marcelampc/d3net_depth_estimation)

<sup>2</sup>[https://github.com/sleekEagle/defocus\\_camind.git](https://github.com/sleekEagle/defocus_camind.git)

TABLE II

RESULTS OF THE ABLATION STUDY. DCC AND ADV DENOTE DARK CHANNEL AS COMPLEMENTARY CUE AND ADVERSARIAL LEARNING, RESPECTIVELY. THE BEST RESULTS ARE IN **BOLD**.

	DCC	ADV	Abs Rel ↓	RMSE↓	$\delta_1\uparrow$	$\delta_2\uparrow$	$\delta_3\uparrow$
①	✓	✓	0.118	0.421	0.825	0.980	0.995
②	✓	✓	0.077	0.362	0.937	0.984	0.995
③	✓		0.066	0.287	0.966	0.992	0.998
★	Ours (full)		<b>0.042</b>	<b>0.240</b>	<b>0.975</b>	<b>0.995</b>	<b>0.999</b>

produces more accurate depth values, particularly at greater distances (fourth row in Fig. 5). This may explain the superior quantitative results shown in Table I. Overall, our method generates visually meaningful results.

We also evaluate the zero-shot generalization capability of our method on real defocused EBD data [25] with entirely different blur magnitudes and extents that were not encountered during training, as shown in Fig. 6. Unlike D3Net [11], the trained model were not fine-tuned on the new dataset. We assume that fine-tuning our model would naturally improve the results on the real dataset. The results in Figs. 6 (b), (c), (e), and (f) demonstrate that our trained model can produce reasonably accurate and more generalizable results than D3Net in zero-shot settings.

### C. Ablation Studies

We report the ablation results on NYU-v2 test data in Table II. The model without the use of dark channel as a complementary cue (DDC) yields the least impressive results (①). Introducing DDC (②) into the model by propagating the concatenated dark channel and defocus RGB image as a 4-channel input through the image encoder, while retaining the LDDCV-Net and MMSP-Net, marks an uptick in performance. In this configuration, D-Net and *Nest(FM)*<sup>2</sup> are excluded. When we train our model without adversarial supervision (③), i.e., without the discriminator, we witness slight degradation in performance as compared to our full model (★).

## IV. CONCLUSION

We have attempted a novel method to infer depth from a single space-variant defocused image. We have investigated the influence of dark channel and its local intensity variation as guidance based on their blur representational features for depth estimation. Experimental results on a realistically modeled synthetic dataset and real defocused data substantiate the potential of our method.

## REFERENCES

- [1] X. Lin, J. Suo, and Q. Dai, “Extracting depth and radiance from a defocused video pair,” *IEEE Trans. Circuits Syst. Video Technol.*, vol. 25, no. 4, pp. 557–569, 2014.
- [2] F. Mannan and M. S. Langer, “Discriminative filters for depth from defocus,” in *Int. Conf. 3D Vis. (3DV)*, 2016, pp. 592–600.
- [3] H. Kumar, A. S. Yadav, S. Gupta, and K. Venkatesh, “Depth map estimation using defocus and motion cues,” *IEEE Trans. Circuits Syst. Video Technol.*, vol. 29, no. 5, pp. 1365–1379, 2018.
- [4] M. Maximov, K. Galim, and L. Leal-Taixé, “Focus on defocus: bridging the synthetic to real domain gap for depth estimation,” in *IEEE Conf. Comput. Vis. Pattern Recognit. (CVPR)*, 2020, pp. 1071–1080.
- [5] Y. Lu, G. Milliron, J. Slagter, and G. Lu, “Self-supervised single-image depth estimation from focus and defocus clues,” *IEEE Robot. Autom. Lett. (RAL)*, vol. 6, no. 4, pp. 6281–6288, 2021.
- [6] G. Song, Y. Kim, K. Chun, and K. M. Lee, “Multi image depth from defocus network with boundary cue for dual aperture camera,” in *IEEE Int. Conf. Acoust. Speech Signal Process. (ICASSP)*, 2020, pp. 2293–2297.
- [7] H. Si, B. Zhao, D. Wang, Y. Gao, M. Chen, Z. Wang, and X. Li, “Fully self-supervised depth estimation from defocus clue,” in *IEEE/CVF Conf. Comput. Vis. Pattern Recognit. (CVPR)*, 2023, pp. 9140–9149.
- [8] Z. Wu, Y. Monno, and M. Okutomi, “Self-supervised spatially variant psf estimation for aberration-aware depth-from-defocus,” in *IEEE Int. Conf. Acoust. Speech Signal Process. (ICASSP)*, 2024, pp. 2560–2564.
- [9] Y. Fujimura, M. Iiyama, T. Funatomi, and Y. Mukaigawa, “Deep depth from focal stack with defocus model for camera-setting invariance,” *Int. J. Comput. Vis.*, vol. 132, no. 6, pp. 1970–1985, 2024.
- [10] S. Anwar, Z. Hayder, and F. Porikli, “Depth estimation and blur removal from a single out-of-focus image,” in *Brit. Mach. Vis. Conf. (BMVC)*, vol. 1, 2017, p. 2.
- [11] M. Carvalho, B. Le Saux, P. Trouvé-Peloux, A. Almansa, and F. Champsagnat, “Deep depth from defocus: how can defocus blur improve 3d estimation using dense neural networks?” in *Eur. Conf. Comput. Vis. (ECCV)*, 2018, pp. 0–0.
- [12] D. Piché-Meunier, Y. Hold-Geoffroy, J. Zhang, and J.-F. Lalonde, “Lens parameter estimation for realistic depth of field modeling,” in *IEEE Conf. Comput. Vis. Pattern Recognit. (CVPR)*, 2023, pp. 499–508.
- [13] L. Wijayasingha, H. Alemzadeh, and J. A. Stankovic, “Camera-independent single image depth estimation from defocus blur,” in *IEEE Winter Conf. Appl. Comput. Vis. (WACV)*, 2024, pp. 3749–3758.
- [14] S. Gur and L. Wolf, “Single image depth estimation trained via depth from defocus cues,” in *IEEE Conf. Comput. Vis. Pattern Recognit. (CVPR)*, 2019, pp. 7683–7692.
- [15] Y. Li, C. Jung, and J. Kim, “Single image depth estimation using edge extraction network and dark channel prior,” *IEEE Access*, vol. 9, pp. 112 454–112 465, 2021.
- [16] K. He, J. Sun, and X. Tang, “Single image haze removal using dark channel prior,” *IEEE Trans. Pattern Anal. Mach. Intell.*, vol. 33, no. 12, pp. 2341–2353, 2010.
- [17] J. Chen and L.-P. Chau, “An enhanced window-variant dark channel prior for depth estimation using single foggy image,” in *IEEE Int. Conf. Image Process. (ICIP)*, 2013, pp. 3508–3512.
- [18] J. Zhou, Q. Liu, Q. Jiang, W. Ren, K.-M. Lam, and W. Zhang, “Underwater camera: Improving visual perception via adaptive dark pixel prior and color correction,” *Int. J. Comput. Vis.*, pp. 1–19, 2023.
- [19] Y. Yan, W. Ren, Y. Guo, R. Wang, and X. Cao, “Image deblurring via extreme channels prior,” in *IEEE Conf. Comput. Vis. Pattern Recognit. (CVPR)*, 2017, pp. 4003–4011.
- [20] J. Pan, D. Sun, H. Pfister, and M.-H. Yang, “Deblurring images via dark channel prior,” *IEEE Trans. Pattern Anal. Mach. Intell.*, vol. 40, no. 10, pp. 2315–2328, 2017.
- [21] J. Cai, W. Zuo, and L. Zhang, “Dark and bright channel prior embedded network for dynamic scene deblurring,” *IEEE Trans. Image Process.*, vol. 29, pp. 6885–6897, 2020.
- [22] N. Silberman, D. Hoiem, P. Kohli, and R. Fergus, “Indoor segmentation and support inference from rgbd images,” in *Eur. Conf. Comput. Vis. (ECCV)*, 2012, pp. 746–760.
- [23] R. Ranftl, K. Lasinger, D. Hafner, K. Schindler, and V. Koltun, “Towards robust monocular depth estimation: Mixing datasets for zero-shot cross-dataset transfer,” *IEEE Trans. Pattern Anal. Mach. Intell.*, vol. 44, no. 3, pp. 1623–1637, 2020.
- [24] D. Haase and M. Amthor, “Rethinking depthwise separable convolutions: How intra-kernel correlations lead to improved mobilenets,” in *IEEE/CVF Conf. Comput. Vis. Pattern Recognit. (CVPR)*, 2020, pp. 14 600–14 609.
- [25] Y. Jin, M. Qian, J. Xiong, N. Xue, and G.-S. Xia, “Depth and dof cues make a better defocus blur detector,” in *IEEE Int. Conf. Multimedia Expo (ICME)*, 2023, pp. 882–887.
- [26] V. Patil, C. Sakaridis, A. Liniger, and L. Van Gool, “P3depth: Monocular depth estimation with a piecewise planarity prior,” in *IEEE Conf. Comput. Vis. Pattern Recognit. (CVPR)*, 2022, pp. 1610–1621.
- [27] B. Ke, A. Obukhov, S. Huang, N. Metzger, R. C. Daudt, and K. Schindler, “Repurposing diffusion-based image generators for monocular depth estimation,” in *IEEE Conf. Comput. Vis. Pattern Recognit. (CVPR)*, 2024, pp. 9492–9502.